© 2016. Published by The Company of Biologists Ltd | Development (2016) 143, 1732-1741 doi:10.1242/dev.126375

RESEARCH ARTICLE

Species-specific contribution of volumetric growth and tissue convergence to posterior body elongation in vertebrates

Ben Steventon[1,*,¶], Fernando Duarte[1,‡], Ronan Lagadec[2,3], Sylvie Mazan[2,3], Jean-François Nicolas[1] and Estelle Hirsinger[1,§]

ABSTRACT

Posterior body elongation is a widespread mechanism propelling the generation of the metazoan body plan. The posterior growth model predicts that a posterior growth zone generates sufficient tissue volume to elongate the posterior body. However, there are energy supply-related differences between vertebrates in the degree to which growth occurs concomitantly with embryogenesis. By applying a multi-scalar morphometric analysis in zebrafish embryos, we show that posterior body elongation is generated by an influx of cells from lateral regions, by convergence-extension of cells as they exit the tailbud, and finally by a late volumetric growth in the spinal cord and notochord. Importantly, the unsegmented region does not generate additional tissue volume. Fibroblast growth factor inhibition blocks tissue convergence rather than volumetric growth, showing that a conserved molecular mechanism can control convergent morphogenesis through different cell behaviours. Finally, via a comparative morphometric analysis in lamprey, dogfish, zebrafish and mouse, we propose that elongation via posterior volumetric growth is linked to increased energy supply and is associated with an overall increase in volumetric growth and elongation.

KEY WORDS: Multi-scalar morphometric analysis, Zebrafish, Mouse, Lamprey, Dogfish, Energy supply

INTRODUCTION

Axial elongation is a widespread mechanism propelling the generation of the metazoan body plan. Despite the importance of this essential event in the formation of the body axis, we know little about the individual cell behaviours driving elongation. This is not surprising given the number of cell behaviours that can lead to the elongation of such a complex, multi-tissue structure. Elongation mechanisms can be separated into two categories. Firstly, those that result in a volumetric increase of the tissue, such as cell growth, deposition of extracellular matrix or a decrease in local density caused by an increase in cell motility, as has been shown in chick (Bénazéraf et al., 2010). Cell proliferation alone (in the absence of cell growth) will not generate volumetric growth. Secondly, those cell behaviours that lead to tissue convergence (i.e. a directional deformation of a tissue in the absence of volumetric growth), such as cell rearrangement, orientated cell division or cell shape change. Vertebrate embryos develop in vastly different nutritive environments that have a large impact on the relative degree of growth occurring during development (O'Farrell, 2015). This is likely to have an impact on the degree to which volumetric growth contributes to elongation. This is especially the case for externally developing embryos with limited energy supply, such as the zebrafish, that must develop a full axis in order to swim and find food prior to overt growth.

A widely accepted model for vertebrate posterior body elongation is that of posterior growth, in which new cells are continually added from the posterior tip of the elongating posterior body. A posterior proliferative zone is thought to drive this process by providing new cells to populate the posterior tissues, the mesoderm and spinal cord in particular (Beddington, 1994; Bouldin et al., 2014; Cambray and Wilson, 2002; Mathis and Nicolas, 2000; McGrew et al., 2008; Nicolas et al., 1996; Selleck and Stern, 1991; Martin and Kimelman, 2010, 2012; Neijts et al., 2014). However, in the absence of growth behaviours, it is not clear whether this posterior proliferative zone can generate sufficient volume increase at the whole structure level to contribute to the elongation of the posterior body. The zebrafish *emi1* (*fbxo5* – Zebrafish Information Network) mutant, in which cell divisions are blocked from the beginning of gastrulation (Riley et al., 2010; Zhang et al., 2008), is shortened by ∼30% but exhibits a non-truncated axis with its full complement of somites. In the scenario in which a posterior proliferative zone would be the major actor, one would expect a truncation of the axis. Several non-growth cell behaviours have been proposed to drive elongation via tissue convergence, particularly in anamniote embryos such as zebrafish. Gastrulation-like cell rearrangements such as convergence-extension, together with novel cellular movements have been observed during zebrafish posterior body elongation (Kanki and Ho, 1997). Blocking fibroblast growth factor (FGF) signalling leads to an inhibition of cellular flow from the tailbud and the disruption of axis elongation (Lawton et al., 2013).

To generate elongation of the posterior body, the posterior growth model predicts that additional tissue volume is generated from the unsegmented region. To address this in zebrafish and to compare with other vertebrates, we aim to determine the relative contribution of volumetric growth (i.e. increase in tissue volume) versus tissue deformation (i.e. elongation in the absence of volume increase) to posterior body elongation. We show that posterior body elongation in zebrafish is generated by an influx of cells from lateral regions, by convergence-extension of cells as they exit the tailbud, and finally by a late volumetric growth in the spinal cord and notochord. The unsegmented region does not generate additional tissue volume. FGF signalling controls convergence within the tailbud and pre-somitic mesoderm (PSM). Our comparative study shows that

[1]Department of Developmental and Stem Cell Biology, Institut Pasteur, 25 rue du Docteur Roux, Paris cedex 15 75724, France. [2]Development and Evolution of Vertebrates, CNRS-UPMC-UMR 7150, Station Biologique, Roscoff 29680, France. [3]CNRS, Sorbonne Universités, UPMC Univ Paris 06, UMR7232, Observatoire Océanologique, Banyuls 66650, France.
*Present address: Department of Genetics, University of Cambridge, Cambridge CB2 3EH, UK. ‡Present address: Centre de Biologie du Développement, UMR 547 CNRS. Universite Paul Sabatiér, 118 Route de Narbonne, Toulouse 31400, France. §Present address: IBPS - Laboratoire de Biologie du Développement (LBD), CNRS, UPMC, UMR 7622, INSERM ERL U1156, 9 Quai Saint-Bernard, Paris Cedex 05 75252, France.

¶Author for correspondence (bjs57@cam.ac.uk)

Received 12 May 2015; Accepted 9 March 2016

Development (2016) 143, 1732-1741 doi:10.1242/dev.126375

posterior volumetric growth is associated with an internal mode of development.

RESULTS

The prospective posterior body is not restricted to the tailbud

Posterior body elongation starts with closure of the primitive streak or blastopore and ends with the completion of somitogenesis. In zebrafish, the anterior body, which corresponds to the anterior trunk, is already established by late gastrula as the anterior trunk somites (1-12) are already present within the pre-somitic mesoderm (Kanki and Ho, 1997). Subsequently, the remaining 20 segments of the body form in an anterior-to-posterior fashion through the process of posterior body elongation, the posterior trunk spanning somites 13-17 and the tail somites 18-32. Previous studies have focused on cells within the tailbud (Kanki and Ho, 1997; Lawton et al., 2013). However, the limits of the posterior body territory are unknown from the end of gastrulation up to the 12-somite stage, when the tailbud has lifted from the yolk and formed a definable prominence. We mapped the limits of the prospective posterior body between the end of gastrulation and the 12-somite stage by generating 12 independent movies in which clusters of 10-20 cells were photolabelled at 90% epiboly and tracked until their incorporation into the embryo axis using Imaris. Photolabelling was achieved with the use of a nuclear-localised KikGR protein (Movie 1), that switches from green to red fluorescence upon UV exposure (Hatta et al., 2006). We find that cells lateral to the tailbud converge and enter the tailbud (Fig. 1A-C, blue). Cells lateral to the elongating axis enter directly into both the spinal cord (Fig. 1A-C, yellow) and the PSM (Fig. 1A-C, red) without having passed through the tailbud (Movie 1).

To determine the extent to which non-tailbud cells contribute to the embryonic axis, we tracked photolabelled cells in movies taken from the lateral view (Movie 2; Fig. 1D-F). Surprisingly, we find that cells contribute to the somitic mesoderm up until the 17th somite, without having first passed through the tailbud region (Movie 2, red tracks; Fig. 1D-F). Cells labelled just caudal to the prospective 17th somite enter into the tailbud prior to the PSM (Movie 2, dark blue tracks; Fig. 1D-F). As somite 17 marks the trunk-tail transition, these results suggest that lateral cells populate the posterior trunk by undergoing convergence and extension without transiting through the tailbud, and that tailbud cells generate the tail only.

To determine whether elongation at these early stages involves cell proliferation, we calculated the proliferation rate within each photolabelled cell clone between the 90% epiboly and 12-somite stages (Fig. 1G). The proliferation rate being ~0.1 cell/h on average, only an average of zero to two additional cells are generated within clones fated towards epidermis, tailbud, spinal cord and the somitic mesoderm, demonstrating that cell proliferation is not a major driving force in early elongation. As a proxy for cell intercalation, we calculated an index of clone dispersion, measured as the mean

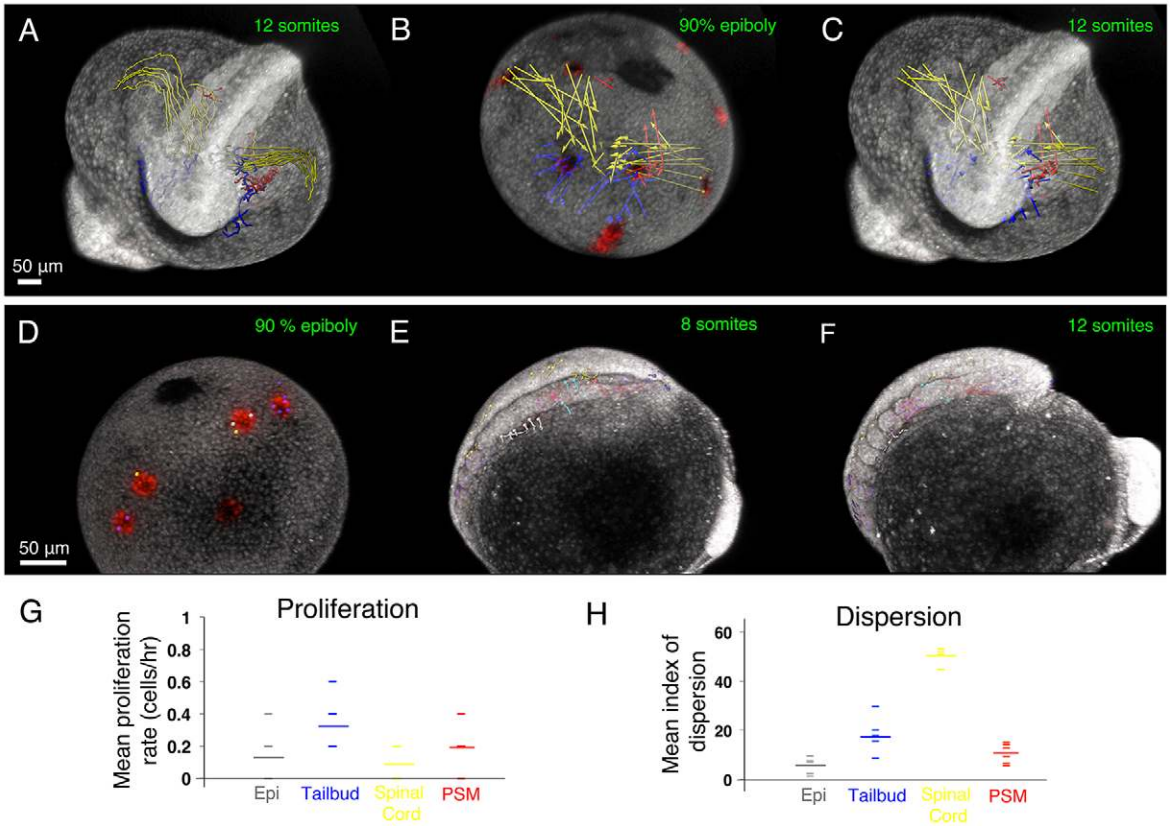

Fig. 1. Convergence of lateral cells contributes to the elongating posterior body. (A-C) Tracks (A) and displacement vectors (B,C) of spinal cord (yellow), tailbud (blue) and PSM (red) precursors from automated tracking of photolabelled nuclei from the 90% epiboly to the 12-somite stage. (D-F) Tracks of cells from the 90% epiboly to the 12-somite stage. (G) Proliferation rate, expressed as the number of additional cells generated divided by the time interval (5 h), within clones fated towards the epidermis (Epi; mean 0.13 cells/h, *n*=53), tailbud (mean 0.36 cells/h, *n*=53), spinal cord (mean 0.04 cells/h, *n*=85) and PSM (mean 0.2 cells/h, *n*=74). (H) Index of dispersion (mean increase in inter-nuclear distance between neighbouring cells) for cells fated towards the epidermis (Epi; mean 5.56 µm, *n*=53), tailbud (mean 18 µm, *n*=53), spinal cord (mean 50 µm, *n*=85) and PSM (mean 11 µm, *n*=74). Small dashes show values from five independent movies. Large dashes mark the mean.

Development (2016) 143, 1732-1741 doi:10.1242/dev.126375

increase in inter-nuclear distance of neighbouring cells between the 90% epiboly and 12-somite stages (Fig. 1H). The index of dispersion is high for all axial clones, particularly for cell clones fated towards the spinal cord (mean increase in internuclear distance: 50 µm), tailbud (18 µm) and PSM (11 µm), with little cell dispersion occurring for the epidermis (5.5 µm). This demonstrates that a considerable degree of cell intercalation is occurring within lateral cells to reach the axial tissues.

Together, these results demonstrate that the prospective posterior body region at late gastrula stage is much larger than previously thought and not restricted to the tailbud, which prompted us to examine the contributions of volumetric growth and tissue deformation at the level of the whole posterior body.

Elongation occurs through extensive convergence with a late phase of volumetric growth

To determine the relative contributions of volumetric growth and tissue deformation to elongation throughout the entire process, we built 3D surface reconstructions of the posterior body and its presumptive territory from the three- to the 32-somite stages using our early fate map and fixed samples at later stages (Fig. 2A; Movie 3). From these, we extracted quantitative information on volume, length, width and height changes. We did not observe an increase in volume until the 24-somite stage (Fig. 2B, grey). However, there is continual elongation despite the absence of volumetric growth (Fig. 2C, grey). Up until the 24-somite stage (Fig. 2D,E, purple to yellow lines), there is a fourfold decrease in width (Fig. 2D) along with an increase in height (Fig. 2E), suggesting that convergence in width is contributing to an increase in both length and height. These results demonstrate that although volumetric growth may contribute to elongation between the 24- and 32-somite stages (growth phase), much of the earlier stages (non-growth phase) of elongation are driven by convergence and extension.

No additional tissue volume is generated from the unsegmented region in zebrafish

We next wanted to determine in which portion of the posterior body volumetric growth is generated: either in the unsegmented region, which includes the tailbud, or within the segmented region. We took embryos previously injected with mRNA encoding cytoplasmic KikGR, photolabelled one or the other region and performed 5 h-long time-lapse imaging (Fig. 3A,D,G; Movie 4). As cells are exiting the tailbud and entering the PSM, we saw considerable mixing of labelled cells with unlabelled cells of the rostral PSM. For our length measurements, we thus took the most anterior and the most posterior photolabelled (i.e. red) cells. For volume measurements, we segmented the photoconverted (i.e. red) signal only. Although the unsegmented region contributes to elongation (2.67-fold increase; Fig. 3B), this region does not increase in volume during both non-growth and growth phases (0.2% decrease in volume; Fig. 3C). We then photolabelled the unsegmented region at the 21-somite stage and measured its volume through to the completion of elongation (Fig. 3D). This further confirmed the absence of unsegmented region volumetric growth during the growth phase (Fig. 3F). However, this region continues to contribute to elongation at these late stages, although to a lesser extent (1.61-fold increase; Fig. 3E). Unlike the unsegmented region, the segmented region (Fig. 3G) does undergo both elongation (2.19-fold increase; Fig. 3H) and volumetric growth (1.25-fold increase; Fig. 3I). Therefore, volumetric growth only occurs in the already segmented region where differentiation is known to take place.

Proliferation rapidly declines in the unsegmented region but continues into the growth phase in the segmented region

We next sought to determine the amount of cell division that occurs within different regions of the posterior body during elongation. To achieve this, we made use of the zFUCCI green transgenic line, which displays green fluorescent nuclei when in S/M/G2 phases of the cell cycle (Sugiyama et al., 2009). We injected these embryos at the one-cell stage with nuclear-localised mCherry mRNA in order to mark all cell nuclei (Fig. 4A). After segmentation of the region of interest, we calculated the percentage of dividing cells as the number of green nuclei over the number of red nuclei in that region. We first analysed the proliferation levels within the entire body (Fig. 4B, black line) or within the tailbud (Fig. 4B, blue line) between the

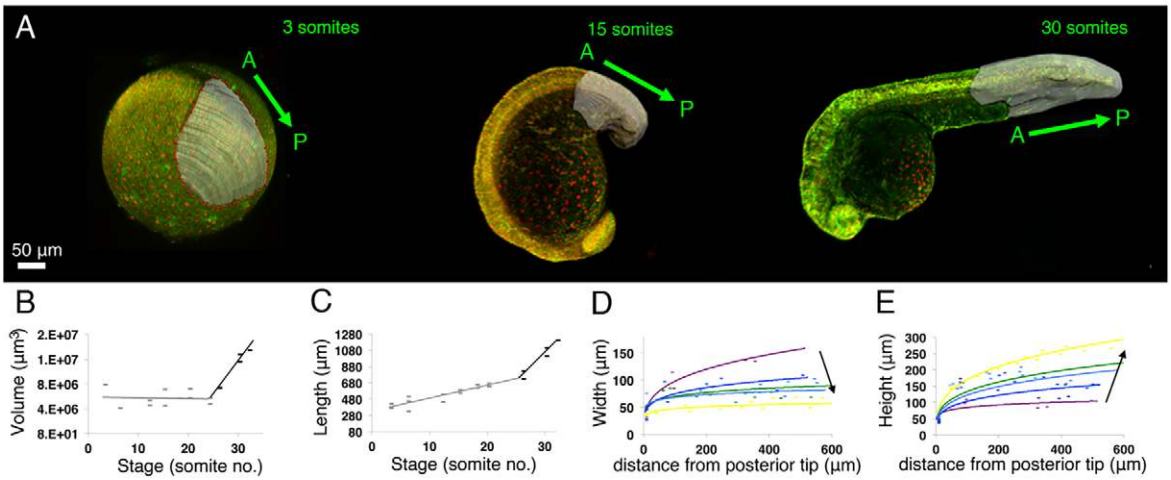

Fig. 2. Posterior body elongation in zebrafish occurs firstly in the absence of volumetric growth followed by a later volumetric growth phase. (A) Surface reconstructions (grey region) of the posterior body through posterior body elongation. Embryos previously injected with nuclear mCherry and membrane eGFP mRNAs in lateral view with A and P marking anterior and posterior poles. (B,C) Plots of volume (B; *n*=21) and length (C; *n*=21) against time (number of somites). Grey points/trendlines: three- to 24-somite stages. Black points/trendlines: 24- to 32-somite stages. (D,E) Width (D) and height (E) against distance from posterior tip of the tail to where each measurement was taken. Each curve corresponds to a developmental stage (number of somites). Colour code: purple, 12 somites (s) (*n*=5); dark blue, 15 s (*n*=8); light blue, 18 s (*n*=7); green, 20 s (*n*=12); yellow, 24 s (*n*=17). Data points show individual measurements; *n*=total number of measurements from three embryos per stage. Black arrows show direction of trend over time.

Development (2016) 143, 1732-1741 doi:10.1242/dev.126375

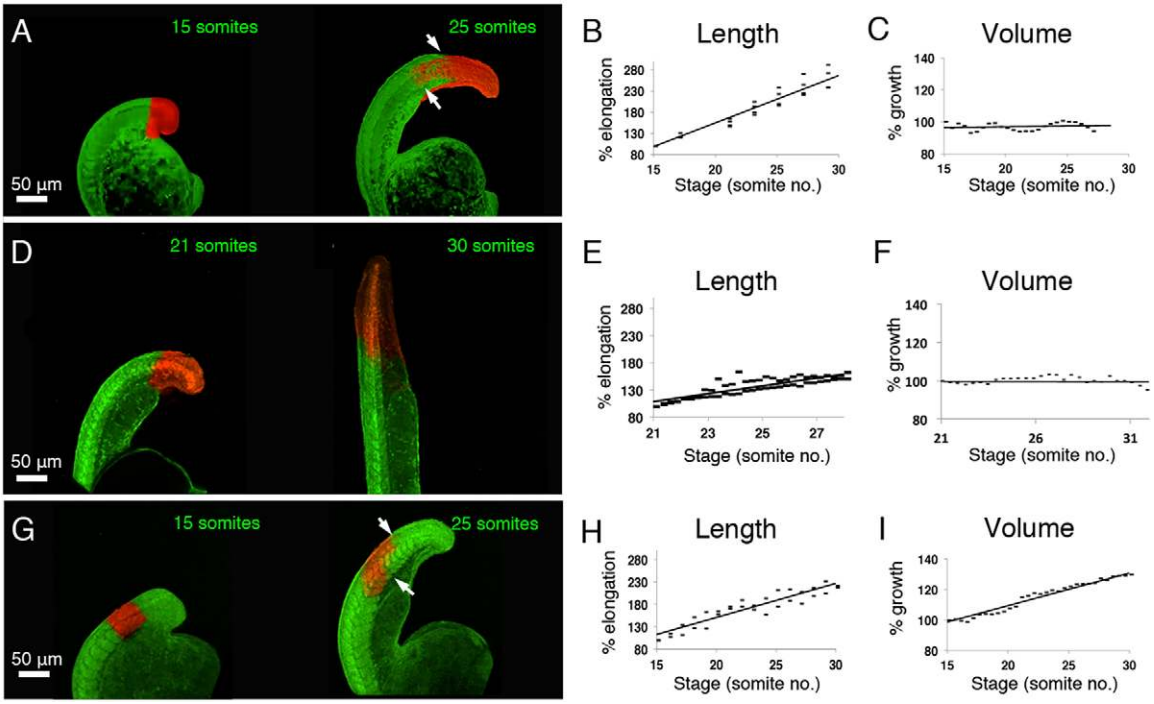

Fig. 3. Volumetric growth only occurs within already segmented regions of the zebrafish posterior body. (A,D,G) Stills from time-lapse movies of embryos injected at the one-cell stage with KikGR mRNA and photolabelled within the unsegmented region at the 15-somite (A) or 21-somite (D) stage or within the segmented region at the 15-somite stage (G). Embryos in lateral view with posterior to the top. (B,E,H) Photoactivated region length (percentage of initial length) plotted against time (number of somites). (B) *n*=25, (E) *n*=51, (I) *n*=29. (C,F,I). Photoactivated region volume (percentage of initial volume) plotted against time (number of somites), (C) *n*=25, (F) *n*=25, (I) *n*=31. White arrows in A and G indicate the displacement of labels within the somitic mesoderm (lower arrows) relative to the spinal cord (upper arrows). Data points show individual measurements; *n*=total number of measurements from three independent experiments.

15- and 22-somite stages. Although at early stages a comparable percentage of cell divisions occurred within the tailbud as with the rest of the posterior body, this dropped off rapidly from the 14-somite stage onwards, similar to what has been reported by Bouldin et al. (2014).

We next evaluated the percentage of dividing cells within the tailbud (Fig. 4C, blue), PSM (Fig. 4C, red), somites (Fig. 4C, orange), spinal cord (Fig. 4C, yellow), notochord (Fig. 4C, purple) and blood precursors (Fig. 4C, green) at the 20-, 25- and 30-somite stages. Only few divisions were observed within the tailbud, and although some cells (~10%) of the PSM are dividing at the 20-somite stage, this rapidly drops as somitogenesis proceeds. Proliferation levels are also low within the notochord, as reported in Sugiyama et al. (2009). By contrast, the proliferation levels within the spinal cord, somites and blood precursors are notably higher. Apart from the early stages of elongation when they are similar, these results show that proliferation levels are higher in the segmented region than in the unsegmented region.

Differential tissue contributions to both volumetric growth and convergence and extension

To assess tissue-specific differences in volumetric growth and convergence, we photolabelled small regions within the tailbud, PSM, somites and spinal cord (Fig. 5A-C) and quantified their

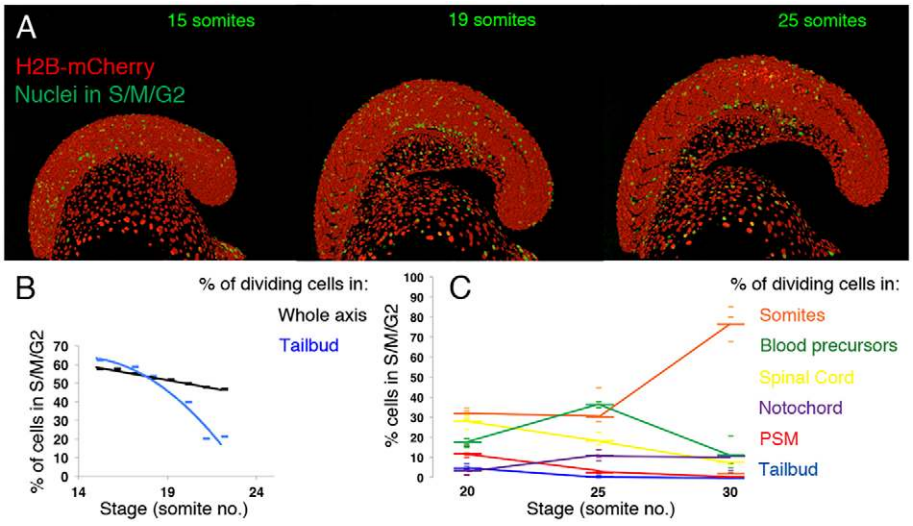

Fig. 4. Proliferation rapidly reaches a low level in the unsegmented region. (A) Stills from a time-lapse of zFUCCI green embryos injected with nuclear mCherry mRNA. (B) Plot of the percentage of nuclei in S/M/G2 (green in A) with respect to total nuclei (red in A) against time (number of somites), showing the posterior body as a whole (black line) and the tailbud (blue line). This trend was observed in three independent time-lapse movies. (C) Percentage of nuclei in S/M/G2 (green) with respect to total nuclei (red) in tailbud (blue), PSM (red), notochord (purple), spinal cord (yellow), blood precursors (green) and somites (orange) at 20-, 25- and 30-somite stages. Small dashes show counts from four embryos fixed at each stage, large dashes indicate mean value.

Development (2016) 143, 1732-1741 doi:10.1242/dev.126375

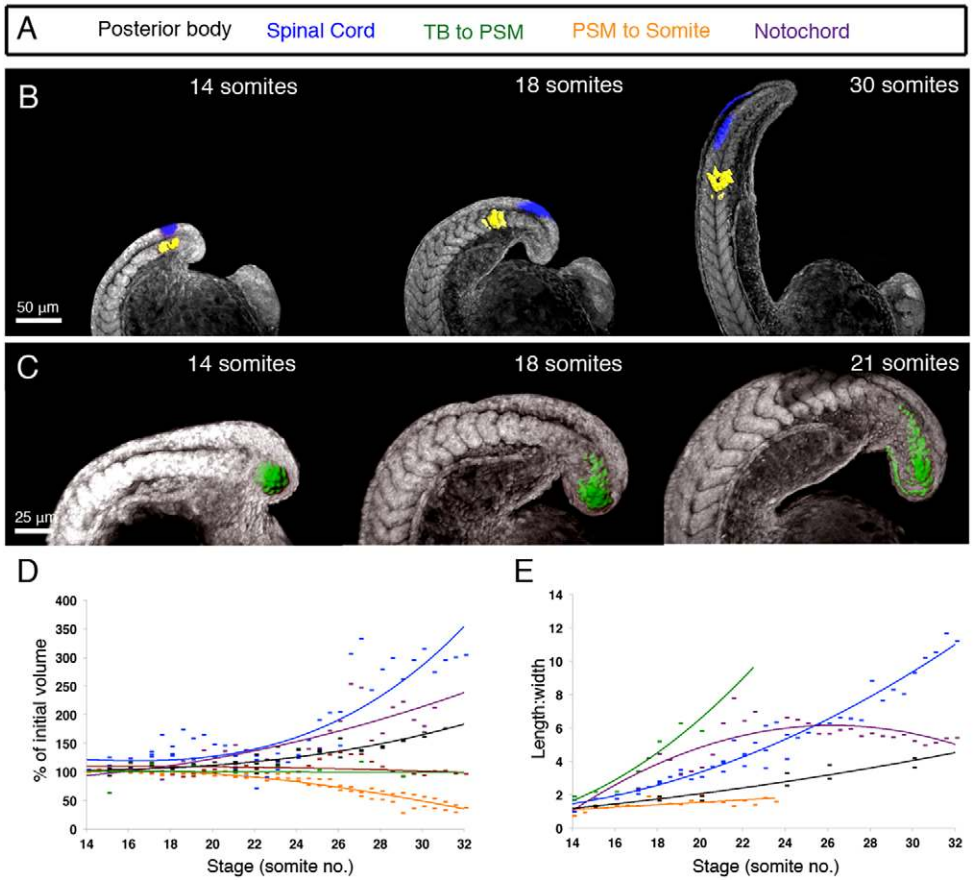

Fig. 5. The spinal cord and notochord are the principal contributors to volumetric growth and the TB-to-PSM transiting cells to thinning and lengthening. (A) Different tissues are colour coded according to the key shown. (B,C) Stills from time-lapse movies of embryos injected at the one-cell stage with KikGR mRNA and photolabelled in the spinal cord and in the PSM (B) or in the tailbud (TB) (C) at the 14-somite stage. (D,E) Plots of volume fold increase (D; spinal cord, *n*=51, notochord; *n*=31; PSM to somites, *n*=58; TB to PSM, *n*=23) and length:width ratio (E; spinal cord, *n*=43; notochord, *n*=30; PSM to somites, *n*=17; TB to PSM, *n*=12) of each photolabelled region against time (number of somites). The red curve in D corresponds to the volume increase of the KikGR-labelled cytoplasm of notochord cells. Data points show individual measurements; *n*=total number of measurements from embryos from three experiments.

percentage of volume increase and their length:width ratio over time (Fig. 5D,E). Compared with the whole posterior body measurements (Fig. 5D,E, black lines), the spinal cord contributes the most to volumetric growth (Fig. 5B,D, blue). This tissue also has a large positive increase in the length:width ratio (Fig. 5B,E, blue; Movie 5, blue), suggesting that either volumetric growth is anisotropic (through oriented cell division or oriented growth of the cells) or that additional cell rearrangements such as convergence-extension are leading to a thinning of this structure. The cells in transit from the tailbud to the PSM contribute the most to thinning and lengthening but in the absence of volumetric growth (Fig. 5C-E, green; Movie 6, green). Once cells have entered the PSM, little thinning and lengthening occurs (Fig. 5B,E, yellow/orange; Movie 5, yellow). This tissue also undergoes a slight compaction during somite formation (Fig. 5B,D, yellow/orange).

Inflation of the notochord by the formation of fluid-filled organelles has an important role in the elongation of the zebrafish axis (Ellis et al., 2013). In line with this, we observe a considerable increase in the volume of bounding-boxes surrounding notochord photolabels (Fig. 5D, purple; includes the organelle volume) without a corresponding increase in the volume of the KikGR-labelled cytoplasm (Fig. 5D, red; excludes the organelle volume). In addition to inflation and proliferation, the notochord also undergoes convergence and extension (Glickman et al., 2003), which is mirrored by an increase in length:width ratio (Fig. 5E, purple). However, as cells begin to inflate, they do so in all directions, leading to a later decrease in length:width ratio (Fig. 5E, purple).

The impact of these distinct tissues on the elongation of the posterior body as a whole will depend on their initial size with respect to the whole posterior body. On embryos previously injected with nuclear mCherry and membrane eGFP mRNAs, we segmented the paraxial mesoderm, spinal cord and notochord at the 15-somite stage and measured their volume as a proportion of the posterior body volume (Fig. S1). The paraxial mesoderm and spinal cord make up the largest portion of the posterior body, at ∼23% and 12%, respectively, confirming their major contribution to elongation. The notochord, at 1.9% of the whole posterior body, contributes to a much lesser extent than the former two tissues. The remaining ∼63% of the posterior body is divided up between inter-tissue components, the non-neural ectoderm, the non-paraxial mesoderm and endodermal tissues which all may be contributing to differing extents to elongation.

FGF signalling is required for convergence and extension, but not posterior volumetric growth in zebrafish

FGF signalling is known to be important for posterior body elongation across vertebrates (Bénazéraf et al., 2010; Bouldin et al., 2014; del Corral and Storey, 2004; Olivera-Martinez et al., 2012; Lawton et al., 2013). We applied our morphometric approach to determine whether FGF signalling plays a role in volumetric growth and/or convergence during posterior body elongation in zebrafish. To circumvent effects on mesoderm induction and patterning as a consequence of inhibiting FGF signalling prior to the end of gastrulation, we added known inhibitors of FGF receptors (SU5402 and PD173074) at the ten-somite stage. Examination at the 32-somite stage revealed clear effects on posterior body morphology compared with DMSO-treated controls (Fig. 6A-D). Neither treatment affected posterior body volume (Fig. 6E; $P>0.7$ in all cases, Student's two-tailed *t*-test). However, we did see a significant reduction in posterior body length (Fig. 6F; $P<0.01$,

Development (2016) 143, 1732-1741 doi:10.1242/dev.126375

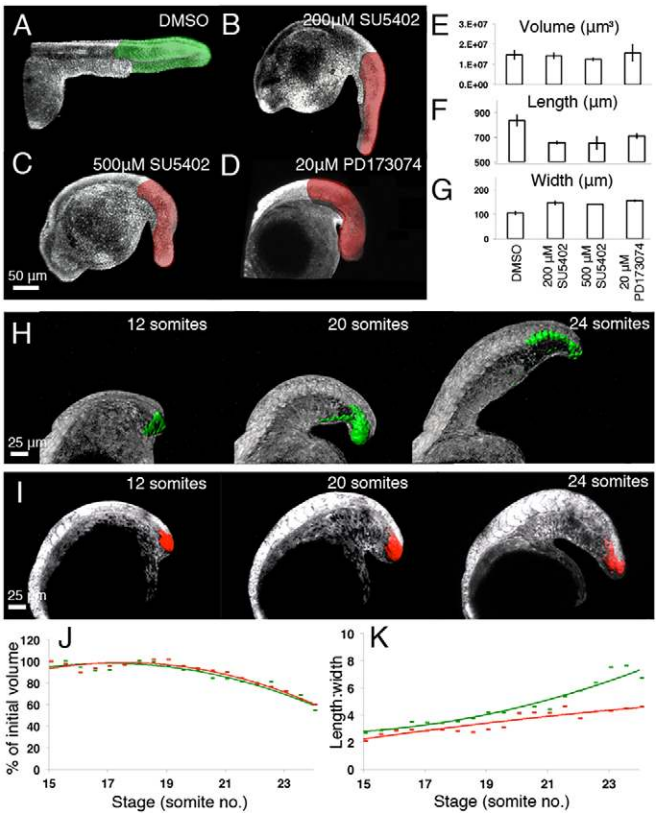

Fig. 6. FGF signalling is required for thinning and lengthening, but not volumetric growth of the zebrafish posterior body. (A-D) Embryos injected at the one-cell stage with nuclear mCherry mRNA and incubated in either 500 µM DMSO (A), 200 µM SU5402 (B), 500 µM SU5402 (C) or 20 µM PD173074 (D) from the ten-somite stage until the 32-somite stage and imaged by confocal microscopy at the 32-somite stage. (E-G) Mean value of posterior body volume (E), length (F) and width (G) for each treatment group at the 32-somite stage. Error bars indicate s.d. (H,I) Stills from time-lapse movies of embryos in which small regions within the tailbud are photolabelled at the 12-somite stage in the presence of 500 µM DMSO (H) or 20 µM PD173074 (I). (J,K) Quantification of the volume (J) and length:width ratio (K) of the photolabelled region over time (number of somites). Green lines correspond to the control situation (500 µM DMSO), red lines indicate treatment with PD173074.

Student's two-tailed *t*-test). This coincided with an increase in mean width (Fig. 6G; $P<0.01$, Student's two-tailed *t*-test), suggesting that an inhibition of convergence and extension is the likely cause of posterior body shortening upon inhibition of FGF signalling. To test this, we repeated our photolabelling of a small region of the tailbud at the 12-somite stage in embryos cultured in DMSO (Fig. 6H) or together with PD173074 (Fig. 6I), and monitored their volume increase and length:width ratio as they transit into the PSM. No effect was observed on the volume of the tailbud photolabelled cells upon addition of PD173074 (Fig. 6J); however, we did observe an inhibition of the length:width ratio increase that is normally observed for these cells (Fig. 6K, compare red and green lines).

To assess whether FGF inhibition is affecting cellular movements and/or cell proliferation/apoptosis, we generated clones of photolabelled cells in the tailbud, PSM or spinal cord at the ten-somite stage (Fig. 7A,C) and quantified their length: width ratio (Fig. 7E) and cell number (Fig. 7F) at the 26-somite stage (Fig. 7B,D) in the absence or presence of SU5402. Although only a slight decrease was observed for cells entering the somites (Fig. 7E, yellow) or within the spinal cord (Fig. 7E, blue), a significant inhibition of the length:width ratio increase for cells that exit the tailbud and enter the PSM was observed upon FGF receptor inhibition (Fig. 7E, red). No effect on cell number was observed for FGF inhibition in any region examined (Fig. 7F). This last result was then confirmed by analysing cell divisions using the zFUCCI line (Fig. 7G-I). SU5402 treatment did not lead to a significant change in the percentage of dividing cells in the entire posterior body at either the 18- or the 32-somite stage (Fig. 7I). Nor did SU5402 treatment affect total cell number with the entire posterior body at either the 18-somite stage (mean cell number=1691±235 for DMSO; 1693±253 for 200 µM SU5402) or the 32-somite stage (mean cell number=2107±359 for DMSO; 2115±441 for 200 µM SU5402). To ensure that our SU5402 treatment adequately blocks FGF signalling, even deep within the tailbud, we made use of a high signal:noise ratio fluorescent *in situ*-based approach (hybridisation chain reaction) that allows for the direct observation of mRNA transcripts by confocal microscopy (Choi et al., 2010, 2014). Staining for *sprouty4* expression as a read-out of FGF signalling activity reveals strong expression in the tailbud (Fig. 7K). Upon addition of SU5402, expression of *sprouty4* is greatly reduced, confirming the efficacy of this small molecule treatment (Fig. 7K). Taken together, these results demonstrate that the role of FGF in zebrafish posterior body elongation is to control tissue convergence as cells exit the tailbud and enter the PSM.

Species-specific contribution of volumetric growth to posterior body elongation in vertebrates

The relatively small contribution of volumetric growth to the elongation of the posterior body in zebrafish is striking and prompted us to determine whether the lack of posterior volumetric growth was characteristic of the external development of anamniote embryos. Therefore we compared our morphometric measurements in zebrafish (Fig. 8C,E) with the amniote mouse embryo (Fig. 8D,E) and with a basal anamniote vertebrate, the lamprey (Fig. 8A,E). As a further comparison, we analysed the anamniote dogfish (Fig. 8B,E), which is evolutionarily basal to teleost fish but develops within an egg case and with a large yolk supply. As long-term photolabelling experiments are not possible in most of these species, we used morphometric measurements of morphological regions on fixed samples as a proxy for quantification of volumetric growth. Embryos for each species were fixed at successive stages between the primitive streak/blastopore closure and the end of somitogenesis, i.e. throughout elongation of the posterior body. We built 3D surface reconstructions and measured volume and length changes of the whole posterior body, the unsegmented region (Fig. 8A-D, red) and the two most anterior body segments (Fig. 8A-D, yellow) of the posterior body.

Both dogfish and mouse embryos showed an initial increase in unsegmented region volume at early stages (Fig. 8B,D). By contrast, in zebrafish and lamprey, this region undergoes a continual reduction in volume throughout elongation (Fig. 8A,C). The measurement of the volume of the two most anterior segments of the posterior body in each species revealed that anterior volumetric growth is occurring in all species, albeit at different intensities that correlate with the intensity of the overall volumetric growth and elongation (Fig. 8H, compare with Fig. 8G and 8F). Taken together, these results demonstrate that although posterior volumetric growth plays a major role in the elongation of the posterior body of both mouse and dogfish embryos, posterior body elongation in both lamprey and zebrafish embryos occurs largely in the absence of posterior volumetric growth.

Development (2016) 143, 1732-1741 doi:10.1242/dev.126375

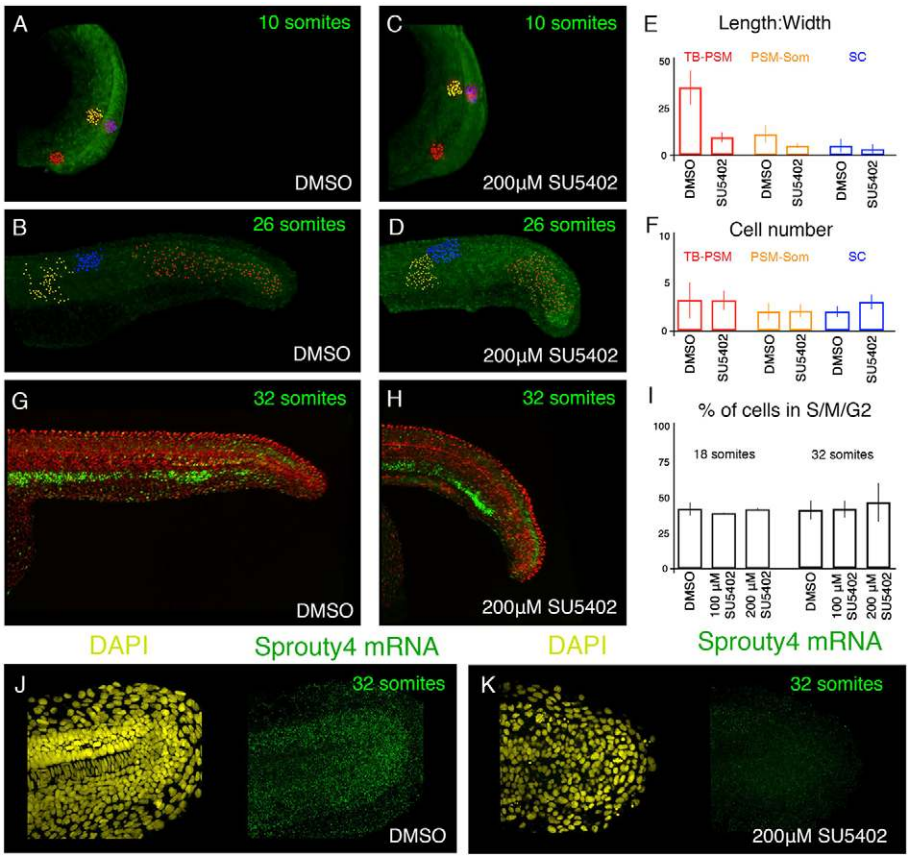

Fig. 7. FGF signalling is required for cell movements but not cell proliferation. (A-D) Embryos previously injected with nls-KikGR mRNA were incubated in either 500 µM DMSO (A,B) or 200 µM SU5402 (C,D). Colours indicate cells in the PSM (yellow), tailbud (red) and spinal cord (blue). (E,F) Photolabels in tailbud (TB-PSM; red), PSM (PSM-Som; yellow) or spinal cord (SC; blue) were measured to display mean length:width ratio (E) and cell number (F). Error bars indicate s.d. (G,H). zFUCCI green embryos injected with nuclear mCherry mRNA and incubated in either 500 µM DMSO (G) or 200 µM SU5402 (H) from the ten- to the 32-somite stage. (I) Mean percentage of nuclei in S/M/G2 are plotted for each treatment group at the 18- and 31-somite stages. Error bars indicate s.d. Three to five embryos were analysed for each condition shown. (J,K) Fluorescent *in situ* hybridisations for the immediate FGF response gene *sprouty4* (green), together with counter-staining for nuclei with DAPI (yellow) in the presence of 200 µM SU5402 (K) or with DMSO only (J). Images are maximum projections of 20× 0.5683 µm *z*-planes through the embryonic midline to determine FGF inhibition deep within the tissue of interest.

Measuring both length and volume changes of the whole posterior body reveals that mice and dogfish, which develop internally, undergo a larger overall elongation and growth than lamprey and zebrafish, which develop externally. This suggests a positive triangular correlation between posterior volumetric growth, overall elongation and volumetric growth, and internal development.

DISCUSSION

Our multi-scalar morphometric and cell-tracking analyses show that posterior body elongation in zebrafish is driven by (1) an influx of cells initially lateral to the elongating posterior body, (2) tissue deformation such as convergence-extension, mostly at the tailbud-PSM transition and (3) volumetric growth in the segmented region, mostly in the spinal cord and notochord. Our comparative analysis suggests that elongation via posterior volumetric growth is linked to an internal mode of development with increased energy supply.

Zebrafish posterior body elongation is not driven by posterior volumetric growth

If posterior growth were a major driver of elongation in zebrafish, one would expect to observe volumetric growth of the unsegmented region. This is not what we observe in our photolabelling experiments. However, we observe that tailbud cells contribute to elongation mostly by rearrangement of pre-existing cells that undergo convergence and extension as they enter the PSM. We do not rule out the existence of slow-dividing self-renewing progenitors that provide cells to the elongating posterior body. What our study shows is that these cells and their derivatives do not generate sufficient additional tissue volume to drive elongation. Our fate mapping shows that a large proportion of the cells that will make up the posterior body come from regions lateral to the elongating posterior body that do or do not transit through the tailbud.

The observation that the segmented region is a major contributor to posterior body elongation explains the bi-phasic growth curve that is observed at the level of the structure as a whole. During the non-growth phase, the spinal cord and notochord volumetric growth, although occurring in anterior trunk structures (data not shown), have not yet begun to occur within the posterior body. However, convergence and extension of cells transiting from the tailbud to the PSM is well underway, resulting in a thinning and lengthening of the posterior body in the absence of volumetric growth. During the growth phase, in addition to continued thinning and lengthening, the dual processes of spinal cord volumetric growth and notochord inflation have reached the posterior body, resulting in an overall increase in posterior body volume and a relative displacement of somitic and spinal cord cells.

Extensive volumetric growth and elongation during embryogenesis are associated with access to a large energy supply

The limited overall and posterior volumetric growth in zebrafish and lamprey is in contrast to both the mouse and dogfish, in which we observe large amounts of volume increase in both unsegmented and segmented regions of the posterior body. The dogfish embryo develops inside an egg case with a large yolk supply that is reminiscent of avian embryos (Sauka-Spengler et al., 2003), and the mouse embryo develops together with a large energy supply from the placenta. This is in contrast to the larval-feeding zebrafish and lamprey embryos that have a limited access to energy and must first establish a full axis in order to swim and find food to grow.

Development (2016) 143, 1732-1741 doi:10.1242/dev.126375

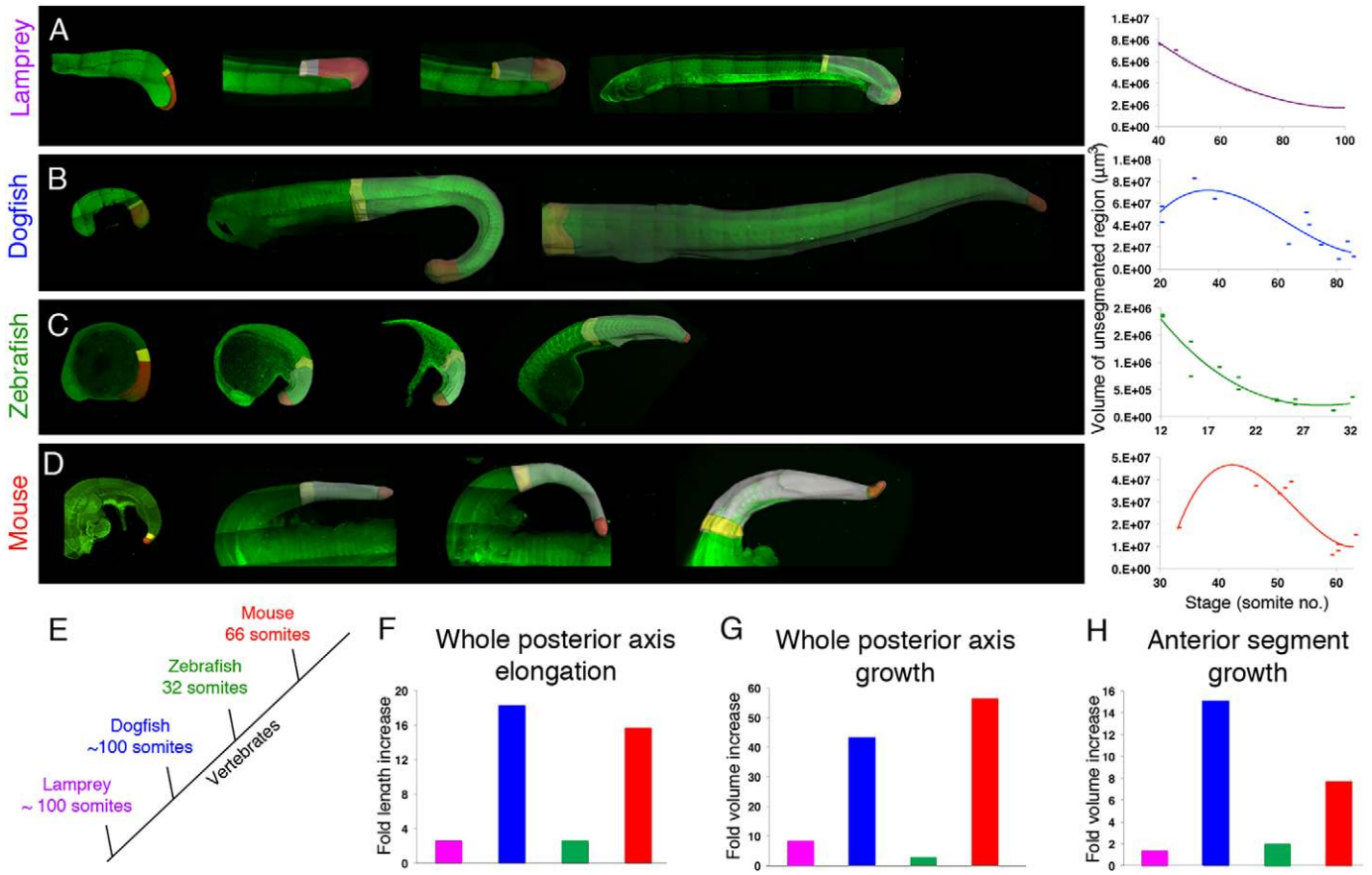

Fig. 8. Comparative 3D morphometric analysis of posterior body elongation across vertebrates. (A-D) Maximal projections of tiled *z*-stacks of lamprey (A; *n*=7), dogfish (B; *n*=11), zebrafish (C; *n*=15) and mouse (D; *n*=10) embryos. All embryos were labelled with DAPI and phalloidin and are shown in lateral view with posterior to the right. Grey surface shows the segmented region, yellow the two most rostral segments of the posterior body and the red surface shows the unsegmented region. Plots of the unsegmented region volume over time (number of somites) are shown to the right for each species. (E) Simplified phylogeny for each species studied together with total somite number. (F-H) Fold change from tailbud stage until the completion of somitogenesis in length (F) and in volume (G) of the whole posterior body and fold change in volume of the two-most anterior segments (H) for each species. Purple bar, lamprey; blue, dogfish; green, zebrafish; red, mouse.

Therefore, overall volumetric growth appears to be associated with the increase in energy that arises from an internal developmental mode. Posterior volumetric growth in dogfish, an anamniote basal to the teleost fish with access to a large energy supply, argues for a direct relationship between an increased maternal energy supply and posterior volumetric growth, rather than for a late emergence of posterior volumetric growth in amniotes. Although tissue deformations are likely to contribute in all cases, an internal mode of development may have allowed for increased contribution of volumetric growth behaviours in embryos such as mouse and dogfish.

Conserved signalling pathways control different cell behaviours according to elongation modes

Despite these differences, there is an apparent conserved requirement for both FGF and Wnt signalling pathway components and downstream Cdx and Brachyury transcription factors for posterior body elongation across a range of vertebrates (Baker et al., 2010; Esterberg and Fritz, 2009; Marlow et al., 2004; Row and Kimelman, 2009; Shimizu et al., 2005; Thorpe, 2005; Yang and Thorpe, 2011). *Brachyury* is also expressed in the tailbud during elongation in dogfish and lamprey embryos (Sauka-Spengler et al., 2003). Furthermore, *Brachyury*, *Wnt3*, *Wnt5* and *Wnt6* are present within the tailbud of amphioxus embryos (Schubert et al., 2001), considered to be the closest living relative of the chordate ancestor (Schubert et al., 2006). A proliferative zone driving body elongation has been identified in several invertebrate embryos and it has been shown to be associated with Wnt signalling in spiders (McGregor et al., 2008), *Artemia* (Copf et al., 2004) and *Tribolium* (Bolognesi et al., 2008; Copf et al., 2004; Schulz et al., 1998). In these different model systems, these signalling pathways are required to direct cell fate decisions and/or to regulate cellular flow as cells exit the tailbud and/or to maintain a posterior growth/proliferative zone. Thus, it is likely that observed conserved molecular mechanisms control different cellular behaviours according to different modes of elongation. In the case of FGF signalling, this pathway has switched from a role in posterior growth/proliferative zone maintenance in amniotes to a role in controlling the cell movements in zebrafish.

MATERIALS AND METHODS

Fish strains and vertebrate embryos

Wild-type AB and zFUCCI green (Tg(EF1α:mAG-zGem(1/100))r^{w0410h} (Sugiyama et al., 2009) embryos were obtained from zebrafish (*Danio rerio*) lines maintained following standard procedures (Westerfield, 2000). Embryos were raised at 28°C and staged according to number of somites. mT/mG double-fluorescent Cre reporter mice were utilised (Muzumdar et al., 2007). Dogfish (*Scyliorhinus canicula*) eggs and lamprey (*Lampetra fluviatilis*) embryos were produced by the Roscoff Marine Station (France). Dogfish and lamprey embryos were staged according to Ballard et al. (1993) and Tahara (1988), respectively.

Development (2016) 143, 1732-1741 doi:10.1242/dev.126375

Preparation and fixation of zebrafish, mouse, dogfish and lamprey samples

Zebrafish wild-type embryos were injected at the one-cell stage with 500 pg of H2B:mCherry and eGFP:CAAX box mRNAs (Hirsinger et al., 2015) and fixed in 4% paraformaldehyde (PFA) for 20 min at room temperature. Dogfish embryos were collected from freshly killed *S. canicula* females and kept in oxygenated sea water at 15°C until dissection and fixation. Lamprey (*L. fluviatilis*) embryos were obtained by *in vitro* fertilisation and incubated at 18°C in oxygenated tap water. Dogfish, lamprey and mouse embryos were fixed overnight in 4% PFA at 4°C and stored at −20°C in 100% methanol, until re-hydration and staining with 1 µg/ml DAPI and 200 nM phalloidin in PBS-0.01% Tween overnight at 4°C.

Imaging of fixed samples

Fixed zebrafish embryos were embedded in 1% low melting point agarose and imaged either on a Zeiss Lightsheet Z.1 microscope or on a Leica SP5 confocal microscope. Lamprey embryos were embedded in 1% low melting point agarose and imaged using a Leica SP5 confocal microscope. Mouse and dogfish embryos were mounted in small chambers containing RapiClear solution (SunJin Lab) and imaged on a Zeiss LSM 7 MP multiphoton microscope. Images were tiled and automatically stitched together using the manufacturer's software.

Zebrafish embryo injections and drug treatment

One-cell stage embryos were injected with 500 pg of the following mRNAs: cytoplasmic KikGR (Hatta et al., 2006), nuclear-targeted nls-KikGR (kind gift of Ian Scott, Department of Molecular Genetics, University of Toronto), nuclear-targeted H2B:mCherry with/without membrane-localised eGFP:CAAX box (Hirsinger et al., 2015). mRNA-injected embryos were incubated in either 500 µM DMSO, 200 µM SU5402, 500 µM SU5402 (Sigma, SML0443-5MG) or 20 µM PD173074 (Sigma, P2499) from the ten- to the 32-somite stage. 90% epiboly or 12-somite stage

Live imaging and mapping of the prospective posterior body

Embryos were embedded in a small drop of 1% low melting point agarose within the central glass ring of a glass-bottomed Petri dish (Mattek; 35 mm Petri dish, 10 mm microwell. No. 1.5 cover glass). The agarose surrounding the tailbud was then removed using a pulled glass capillary and imaged on an inverted Leica SP5 confocal microscope with a 20× air objective. Ten to 20 nuclei were photoconverted from green to red by exposing the cells to ten 200 Hz scans of a 405 laser at 60× zoom. Nuclei were tracked in 4D using the image analysis tool Imaris (Andor Technology). Tracks were filtered to include tracks from 90% epiboly through to the 12-somite stage and manually corrected. Surface renderings were automatically segmented on the green channel using the 'surface' tool in Imaris, and reference points were added at 50-µm intervals along the embryonic midline from the dorsal blastopore. Two lines were measured from these reference points to tracks located at a boundary either between the posterior body-fated cells and the non-axial epidermis, or between posterior body-fated cells and anterior trunk-fated cells. Three- and six-somite-stage embryos imaged by light-sheet microscopy were used to map the full complement of boundary points with the use of midline reference points as described. Surface reconstructions were created by manually drawing contours at 10-µm intervals.

Volume segmentation and morphometric analysis

To segment posterior body volume we utilised the 'Manually create surface' function of Imaris. Contours were manually drawn at 10-µm intervals in the *z*-plane, bordering the last-formed anterior trunk somite boundary of each species (somite 12 for zebrafish, 33 for mouse, 40 for lamprey and 20 for dogfish; Richardson et al., 1998). For unsegmented regions, we took everything posterior to the notochord. For the anterior body segments, we used the somite boundary of the first two posterior body somites. Measurement points were placed at every other somite boundary along the axis, and the values summed to give the length of the posterior body at any given stage. Height and width measurements were made at each length measurement point and plotted as described in the main text.

For the photolabelling experiments, embryos were imaged as for the cell-tracking experiments. Surface renderings were automatically created based on the red channel at consecutive stages through the movies. Volume, height and width measurements were made as described above.

Cell counts and calculation of index of dispersion

All nuclei within each image stack were segmented using the Imaris 'Spots' function. Manually checking the segmentation revealed that a diameter of 4 µm enabled the optimum segmentation of all nuclei in the image. Individual nuclei of clones labelled by photoconverting nls-KikGR were segmented as described above for cell counts. For each nucleus, the distance to all other nuclei along *x*-, *y*- and *z*-axes was calculated and ordered. The mean distance of the six closest neighbours was calculated for each nucleus within the cluster and the mean change calculated as the index of dispersion for each labelled clone.

Quantification of the proliferation levels in zFUCCI green embryos

zFUCCI green embryos were injected with nuclear mCherry mRNA at the one-cell stage and imaged as described above. At the formation of each additional somite between the 12- and 20-somite stages, both the whole posterior body and tailbud (determined as the undifferentiated region of the body posterior to the notochord) were segmented in 3D as described above. For tissue-specific counts, we first generated tissue-specific surface renderings from manually drawn contours at 10-µm intervals through the *z*-stack. These were then taken as 'cells' in the Imaris 'Cell' to count both total nuclei (using the H2B:mCherry signal) and nuclei in S/M/G2 (using the zFUCCI green signal) within each tissue region. Nuclei were automatically detected using the Imaris 'Spots' function and manually inspected for accuracy.

Hybridisation chain reaction for assessing *sprouty4* expression

Five antisense DNA probes were designed against the full length zebrafish *sprouty4* mRNA sequence (accession number NM_131826.1) as described by Choi et al. (2014). Embryos incubated in either DMSO or with 200 µM SU5402 from the ten-somite to the 32-somite stage were fixed overnight in 4% PFA at 4°C and then stained according to Choi et al. (2014). Imaging was performed on a Zeiss 700 confocal microscope with identical imaging parameters: *z*-step 0.5683 µm; 1024×1024 resolution; 63× oil objective; 35% laser power at 488 nm; gain 661; digital offset −2; pixel dwell time 3.12 µm.

Acknowledgements

We would like to thank Alfonso Martinez-Arias for critical reading of the manuscript and Eric Theveneau, Simon Restrepo, Claire Fournier-Thibault and Carlos Carmona-Fontaine for further essential commentary. We are indebted to Pascal Dardenne for excellent animal care and Christine Chevalier for help in isolating mouse embryos. We would like to thank Nicolas David and Florence Giger (IBENS, Paris) for kindly hosting some of the zFucci-related experiments. We would also like to thank Ian Scott for the gift of the nls-KikGR construct. Finally, we acknowledge the Plateforme d'Imagerie Dynamique, Institut Pasteur, for their excellent imaging service and support.

Competing interests

The authors declare no competing or financial interests.

Author contributions

B.S., E.H. and J.-F.N. conceived the project. B.S. performed most of the experiments and developed analytical assays. F.D. aided in performing morphometric measurements. E.H. performed live imaging for gastrula-stage fate maps. R.L. and S.M. aided in staging and obtaining lamprey and dogfish embryos. B.S. and E.H. interpreted the results. B.S. and E.H. wrote the paper.

Funding

This work was funded by the Institut Pasteur (J.-F.N. and E.H.; a Roux fellowship to B.S.); a grant from the Agence Nationale de la Recherche [ANR-10-BLAN-121801 DEVPROCESS to J.-F.N., E.H. and B.S.]; the Centre National de la Recherche Scientifique (CNRS) (E.H. and S.M.); the Institut National de la Santé et de la Recherche Médicale (INSERM) (J.-F.N.); and a fellowship from the French Muscular Dystrophy Association (AFM-Téléthon) [number 16829 to B.S.].

Development (2016) 143, 1732-1741 doi:10.1242/dev.126375

Supplementary information

Supplementary information available online at
http://dev.biologists.org/lookup/suppl/doi:10.1242/dev.126375/-/DC1

References

Baker, K. D., Ramel, M.-C. and Lekven, A. C. (2010). A direct role for Wnt8 in ventrolateral mesoderm patterning. *Dev. Dyn.* **239**, 2828-2836.

Ballard, W. W., Mellinger, J. and Lechenault, H. (1993). A series of normal stages for development of Scyliorhinus canicula, the lesser spotted dogfish (Chondrichthyes: Scyliorhinidae). *J. Exp. Zool.* **267**, 318-336.

Beddington, R. S. (1994). Induction of a second neural axis by the mouse node. *Development* **120**, 613-620.

Bénazéraf, B., François, P., Baker, R. E., Denans, N., Little, C. D. and Pourquié, O. (2010). A random cell motility gradient downstream of FGF controls elongation of an amniote embryo. *Nature* **466**, 248-252.

Bolognesi, R., Farzana, L., Fischer, T. D. and Brown, S. J. (2008). Multiple Wnt genes are required for segmentation in the short-germ embryo of Tribolium castaneum. *Curr. Biol.* **18**, 1624-1629.

Bouldin, C. M., Snelson, C. D., Farr, G. H. and Kimelman, D. (2014). Restricted expression of cdc25a in the tailbud is essential for formation of the zebrafish posterior body. *Genes Dev.* **28**, 384-395.

Cambray, N. and Wilson, V. (2002). Axial progenitors with extensive potency are localised to the mouse chordoneural hinge. *Development* **129**, 4855-4866.

Choi, H. M. T., Chang, J. Y., Trinh, L. A., Padilla, J. E., Fraser, S. E. and Pierce, N. A. (2010). Programmable in situ amplification for multiplexed imaging of mRNA expression. *Nat. Biotechnol.* **28**, 1208-1212.

Choi, H. M. T., Beck, V. A. and Pierce, N. A. (2014). Next-generation in situ hybridization chain reaction: higher gain, lower cost, greater durability. *ACS Nano.* **8**, 4284-4294.

Copf, T., Schröder, R. and Averof, M. (2004). Ancestral role of caudal genes in axis elongation and segmentation. *Proc. Natl. Acad. Sci. USA* **101**, 17711-17715.

del Corral, R. D. and Storey, K. G. (2004). Opposing FGF and retinoid pathways: a signalling switch that controls differentiation and patterning onset in the extending vertebrate body axis. *Bioessays* **26**, 857-869.

Ellis, K., Hoffman, B. D. and Bagnat, M. (2013). The vacuole within: how cellular organization dictates notochord function. *Bioarchitecture* **3**, 64-68.

Esterberg, R. and Fritz, A. (2009). dlx3b/4b are required for the formation of the preplacodal region and otic placode through local modulation of BMP activity. *Dev. Biol.* **325**, 189-199.

Glickman, N. S., Kimmel, C. B., Jones, M. A. and Adams, R. J. (2003). Shaping the zebrafish notochord. *Development* **130**, 873-887.

Hatta, K., Tsujii, H. and Omura, T. (2006). Cell tracking using a photoconvertible fluorescent protein. *Nat. Protoc.* **1**, 960-967.

Hirsinger, E., Carvalho, J. E., Chevalier, C., Lutfalla, G., Nicolas, J. F., Peyriéras, N. and Schubert, M. (2015). Expression of fluorescent proteins in Branchiostoma lanceolatum by mRNA injection into unfertilized oocytes. *J. Vis. Exp.* **95**, 52042.

Kanki, J. P. and Ho, R. K. (1997). The development of the posterior body in zebrafish. *Development* **124**, 881-893.

Lawton, A. K., Nandi, A., Stulberg, M. J., Dray, N., Sneddon, M. W., Pontius, W., Emonet, T. and Holley, S. A. (2013). Regulated tissue fluidity steers zebrafish body elongation. *Development* **140**, 573-582.

Marlow, F., Gonzalez, E. M., Yin, C., Rojo, C. and Solnica-Krezel, L. (2004). No tail co-operates with non-canonical Wnt signaling to regulate posterior body morphogenesis in zebrafish. *Development* **131**, 203-216.

Martin, B. L. and Kimelman, D. (2010). Brachyury establishes the embryonic mesodermal progenitor niche. *Genes Dev.* **24**, 2778-2783.

Martin, B. L. and Kimelman, D. (2012). Canonical Wnt signaling dynamically controls multiple stem cell fate decisions during vertebrate body formation. *Dev. Cell* **22**, 223-232.

Mathis, L. and Nicolas, J. F. (2000). Different clonal dispersion in the rostral and caudal mouse central nervous system. *Development* **127**, 1277-1290.

McGregor, A. P., Pechmann, M., Schwager, E. E., Feitosa, N. M., Kruck, S., Aranda, M. and Damen, W. G. M. (2008). Wnt8 is required for growth-zone establishment and development of opisthosomal segments in a spider. *Curr. Biol.* **18**, 1619-1623.

McGrew, M. J., Sherman, A., Lillico, S. G., Ellard, F. M., Radcliffe, P. A., Gilhooley, H. J., Mitrophanous, K. A., Cambray, N., Wilson, V. and Sang, H. (2008). Localised axial progenitor cell populations in the avian tail bud are not committed to a posterior Hox identity. *Development* **135**, 2289-2299.

Muzumdar, M. D., Tasic, B., Miyamichi, K., Li, L. and Luo, L. (2007). A global double-fluorescent Cre reporter mouse. *Genesis* **45**, 593-605.

Neijts, R., Simmini, S., Giuliani, F., van Rooijen, C. and Deschamps, J. (2014). Region-specific regulation of posterior axial elongation during vertebrate embryogenesis. *Dev. Dyn.* **243**, 88-98.

Nicolas, J. F., Mathis, L., Bonnerot, C. and Saurin, W. (1996). Evidence in the mouse for self-renewing stem cells in the formation of a segmented longitudinal structure, the myotome. *Development* **122**, 2933-2946.

O'Farrell, P. H. (2015). Growing an Embryo from a Single Cell: A Hurdle in Animal Life. *Cold Spring Harb. Persp. Biol.* **7**, a019042.

Olivera-Martinez, I., Harada, H., Halley, P. A. and Storey, K. G. (2012). Loss of FGF-dependent mesoderm identity and rise of endogenous retinoid signalling determine cessation of body axis elongation. *PLoS Biol.* **10**, e1001415.

Richardson, M. K., Allen, S. P., Wright, G. M., Raynaud, A. and Hanken, J. (1998). Somite number and vertebrate evolution. *Development* **125**, 151-160.

Riley, B. B., Sweet, E. M., Heck, R., Evans, A., McFarland, K. N., Warga, R. M. and Kane, D. A. (2010). Characterization of harpy/Rca1/emi1 mutants: patterning in the absence of cell division. *Dev. Dyn.* **239**, 828-843.

Row, R. H. and Kimelman, D. (2009). Bmp inhibition is necessary for post-gastrulation patterning and morphogenesis of the zebrafish tailbud. *Dev. Biol.* **329**, 55-63.

Sauka-Spengler, T., Baratte, B., Lepage, M. and Mazan, S. (2003). Characterization of Brachyury genes in the dogfish S. canicula and the lamprey L. fluviatilis. Insights into gastrulation in a chondrichthyan. *Dev. Biol.* **263**, 296-307.

Schubert, M., Holland, L. Z., Stokes, M. D. and Holland, N. D. (2001). Three amphioxus Wnt genes (AmphiWnt3, AmphiWnt5, and AmphiWnt6) associated with the tail bud: the evolution of somitogenesis in chordates. *Dev. Biol.* **240**, 262-273.

Schubert, M., Escriva, H., Xavier-Neto, J. and Laudet, V. (2006). Amphioxus and tunicates as evolutionary model systems. *Trends Ecol. Evol.* **21**, 269-277.

Schulz, C., Schröder, R., Hausdorf, B., Wolff, C. and Tautz, D. (1998). A caudal homologue in the short germ band beetle Tribolium shows similarities to both, the Drosophila and the vertebrate caudal expression patterns. *Dev. Genes Evol.* **208**, 283-289.

Selleck, M. A. and Stern, C. D. (1991). Fate mapping and cell lineage analysis of Hensen's node in the chick embryo. *Development* **112**, 615-626.

Shimizu, T., Bae, Y.-K., Muraoka, O. and Hibi, M. (2005). Interaction of Wnt and caudal-related genes in zebrafish posterior body formation. *Dev. Biol.* **279**, 125-141.

Sugiyama, M., Sakaue-Sawano, A., Iimura, T., Fukami, K., Kitaguchi, T., Kawakami, K., Okamoto, H., Higashijima, S.-i. and Miyawaki, A. (2009). Illuminating cell-cycle progression in the developing zebrafish embryo. *Proc. Natl. Acad. Sci. USA* **106**, 20812-20817.

Tahara, Y. (1988). Normal stages of development in lamprey, Lampetra reissneri (Dybowski). *Zoolog. Sci.* **5**, 109-118.

Thorpe, C. J. (2005). Wnt/β-catenin regulation of the Sp1-related transcription factor sp5l promotes tail development in zebrafish. *Development* **132**, 1763-1772.

Westerfield, M. (2000). *The Zebrafish Book: A Guide for the Laboratory Use of Zebrafish (Danio rerio)*. Eugene, OR: University of Oregon Press.

Yang, Y. and Thorpe, C. (2011). BMP and non-canonical Wnt signaling are required for inhibition of secondary tail formation in zebrafish. *Development* **138**, 2601-2611.

Zhang, L., Kendrick, C., Jülich, D. and Holley, S. A. (2008). Cell cycle progression is required for zebrafish somite morphogenesis but not segmentation clock function. *Development* **135**, 2065-2070.